Universitat Politècnica de Catalunya (UPC)
Universitat Autònoma de Barcelona (UAB)
Universitat de Barcelona (UB)
Institut de Ciències Fotòniques (ICFO)

http://www.photonicsbcn.eu

Master in Photonics

MASTER THESIS WORK

OPTICAL SUPER-RESOLUTION TECHNIQUES FOR 3D PROFILOMETRY

Olena Zhukova

Supervised by Dr. Guillem Carles Santacana (Sensofar-Tech) and Prof. Santiago Royo Royo (UPC)

Presented on date 1st September 2021

Registered at

Escola Tècnica Superior d'Enginyeria de Telecomunicació de Barcelona

Optical super-resolution techniques for 3D profilometry

Olena Zhukova
R&D Department, Sensofar-Tech, S.L., Ctra. BV- 1274, km 1, 08225 Terrassa, Spain

E-mail:

Abstract. The resolution of conventional 3D optical profilometers is limited by diffraction, characterized by the numerical aperture (NA) of the objective and the wavelength of the light source used for imaging. To resolve structures with resolution beyond this limit, super-resolution techniques must be used. In this thesis two super-resolution techniques were evaluated, Structured Illumination microscopy (SIM) and Fourier Ptychographic microscopy (FPM), by modifying the acquisition process of already existing profilometry systems provided by Sensofar. The modifications allowed to acquire the datasets necessary to run the reconstruction algorithms for both techniques, which were built to generate higher resolution images as output. The FPM algorithm was also tested on open-source datasets, while the performance of the SIM algorithm was compared to the results of an open-source algorithm.

Keywords: Structured illumination, Fourier ptychography, super-resolution, surface metrology.

1. Introduction

Going beyond the diffraction limit of light, once thought to be an unbreakable physical limit, is now a necessity in numerous fields. In biomedical research super-resolution allows to visualize molecules at nanometric scale, while in 3D surface metrology high-resolution imaging is performed by using high NA objectives, which also allow imaging of surfaces with large slopes. Various techniques have been developed to enhance resolution, being based on point spread function engineering such as STED microscopy or on single-molecule localization such as PALM or STORM. These techniques rely on fluorescence and require high-powered light sources, which makes them difficult to implement as add-on modules into existing surface metrology systems.
The object of this thesis is to assess the performance of two super-resolution techniques not reliant on fluorescence by implementing them into 3D optical profilers already available on the market. These techniques, called Structured Illumination microscopy (SIM) and Fourier Ptychography microscopy (FPM), combine image acquisition and image processing to achieve a resolution beyond the diffraction limit by expanding the frequency spectrum. Despite both techniques relying heavily on computational post-processing of the experimental data, their execution in image acquisition and image reconstruction algorithms are vastly different.

1.1. SIM principle

Imaging systems can be characterized by the optical transfer function (OTF), which represents the ability of the optical system to transfer different spatial frequencies. The OTF decays smoothly until reaching zero for a given frequency called the cutoff frequency, proportional to the ratio between the objective NA and the wavelength of the light source. No frequencies beyond this limit can be transmitted by the optical system.
During acquisition, all high frequency information beyond the cutoff is lost due to the finite size of the imaging system's aperture. Imaging is equivalent to multiplying the Fourier spectrum of a surface by the OTF, thus suppressing the highest frequencies and removing all frequencies beyond the cutoff. This dictates the maximum resolution, as high frequencies correspond to fine structures on a surface. SIM provides enhanced lateral resolution by artificially increasing the width of the

OTF, thus allowing higher frequencies to be reconstructed. It exploits the Moiré effect to make detectable those spatial frequencies that were previously inaccessible, by moving them into the support region of the imaging system [1].

The Moiré effect appears when two sinusoidal patterns are superposed, and it can be understood as the appearance of a "beat" pattern, of lower frequency than the patterns that compose it. Similarly, a Moiré effect can be observed when a periodic pattern is projected onto a surface containing fine details. In such case frequency mixing occurs; additional frequency components are brought into the OTF's spatial frequency range, and the Moiré fringes encode information both about the structured illumination and the high-frequency components of the surface. By knowing the characteristics of the projected illumination pattern, it is possible to unmix the frequencies and recover the information pertaining to the surface [2].

Spatial frequencies beyond the optical cutoff that are mixed within the OTF support cannot be separated from the original information by only using one image because the phase of each spatial frequency must be recovered as well. Due to this, a few images with different phase shifts of the illumination patterns are used, usually three images with equally spaced phase shifts. To cover a larger region of the 2D Fourier space the patterns are projected in multiple directions, which allows for a more isotropic reconstruction.

Structured illumination used in SIM can be represented by a sinusoidal function, described by (1),

$$I_{\theta,\phi}(\boldsymbol{r}) = I_o[1 - m\cos(2\pi \boldsymbol{p}_\theta \cdot \boldsymbol{r} + \phi)] \tag{1}$$

where $\boldsymbol{r} \equiv (x, y)$ is the spatial position vector, I_o is the maximum illumination intensity, m the modulation factor, $\boldsymbol{p}_\theta = (p\,cos\theta, p\,sin\theta)$ the illumination frequency vector in reciprocal space, with θ being the orientation of the sinusoidal pattern and ϕ is the phase.

After acquisition, the intensity of an image in the image plane can be defined by (2),

$$D_{\theta,\phi}(\boldsymbol{r}) = \left[S(\boldsymbol{r}) I_{\theta,\phi}(\boldsymbol{r})\right] \otimes H(\boldsymbol{r}) \tag{2}$$

where $S(\boldsymbol{r})$ represents the surface distribution of the sample and $H(\boldsymbol{r})$ the optical system's PSF. The Fourier transform of this image is given by (3), where $\tilde{H}(\mathbf{k})$ represents the system's OTF.

$$\tilde{D}_{\theta,\phi}(\mathbf{k}) = \left[\tilde{I}_{\theta,\phi}(\mathbf{k}) \otimes \tilde{S}(\mathbf{k})\right] \cdot \tilde{H}(\mathbf{k}) = I_o\left[\tilde{S}(\mathbf{k}) - \frac{m}{2}\tilde{S}(\mathbf{k} - \mathbf{p}_\theta)e^{-i\phi} - \frac{m}{2}\tilde{S}(\mathbf{k} + \mathbf{p}_\theta)e^{i\phi}\right] \cdot \tilde{H}(\mathbf{k}) \tag{3}$$

Equation (3) shows that the Fourier transform of the captured image corresponds to a linear combination of three different regions limited by the support of the OTF, centered at the origin, $\boldsymbol{p}_\theta$ and $-\boldsymbol{p}_\theta$, respectively. If the frequency vector and the phases of the illumination pattern are known, it is possible to recover the information about the surface modulated by the OTF by solving the set of linear equations given by (4).

$$\begin{bmatrix} \tilde{S}(\mathbf{k})\tilde{H}(\mathbf{k}) \\ \tilde{S}(\mathbf{k} - \mathbf{p}_\theta)\tilde{H}(\mathbf{k}) \\ \tilde{S}(\mathbf{k} + \mathbf{p}_\theta)\tilde{H}(\mathbf{k}) \end{bmatrix} = \mathbf{M}^{-1} \begin{bmatrix} \tilde{D}_{\theta,\phi_1}(\mathbf{k}) \\ \tilde{D}_{\theta,\phi_2}(\mathbf{k}) \\ \tilde{D}_{\theta,\phi_3}(\mathbf{k}) \end{bmatrix}, \quad \text{with } \mathbf{M} = \begin{matrix} 1 & -\frac{m}{2}e^{-i\phi_1} & -\frac{m}{2}e^{+i\phi_1} \\ 1 & -\frac{m}{2}e^{-i\phi_2} & -\frac{m}{2}e^{+i\phi_2} \\ 1 & -\frac{m}{2}e^{-i\phi_3} & -\frac{m}{2}e^{+i\phi_3} \end{matrix} \tag{4}$$

One equation is solved for each pattern orientation θ. To recover the surface information a simple division by $\tilde{H}(\mathbf{k})$ would greatly amplify the noise for the frequencies where the OTF approaches zero. To avoid this problem a Wiener filter is applied instead, which maintains the balance between resolution enhancement and noise suppression. One such filter is applied to the central frequency component and another to the side frequency components, given by (5) and (6).

$$\tilde{S}_u(\mathbf{k}) = \left[\frac{\tilde{H}^*(\mathbf{k})}{|\tilde{H}(\mathbf{k})|^2 + w_c}\right]\tilde{S}(\mathbf{k})\tilde{H}(\mathbf{k}) \tag{5}$$

$$\tilde{S}_u(\mathbf{k} \pm \mathbf{p}_\theta) = \frac{1}{m}\left[\frac{\tilde{H}^*(\mathbf{k})}{|\tilde{H}(\mathbf{k})|^2 + w_s}\right]\tilde{S}(\mathbf{k} \pm \mathbf{p}_\theta)\tilde{H}(\mathbf{k}) \tag{6}$$

Wiener filters are characterized by Wiener parameters, w_c and w_s, proportional to the inverse of the SNR. Their values must be adjusted empirically.

The separated frequency components can be now shifted to their correct location in the Fourier spectrum by making use of the Fourier shift theorem given by (7),

$$\tilde{S}_s(\mathbf{k} \pm \mathbf{p}_\theta) = \mathcal{F}\left[\mathcal{F}^{-1}\{\tilde{S}_u(\mathbf{k} \pm \mathbf{p}_\theta)\} \times e^{\pm i2\pi(\mathbf{p}_\theta \cdot \mathbf{r})}\right] \tag{7}$$

where $\mathcal{F}$ and $\mathcal{F}^{-1}$ denote the Fourier transform and the inverse Fourier transform, respectively.

The final reconstruction of the Fourier spectrum is performed by weighted averages, making use of a generalized Wiener filter, shown in (8),

$$\widetilde{D}_{\mathrm{SIM}}(\mathbf{k}) = \sum_{\theta=\theta_1}^{\theta_3} \frac{|\widetilde{H}(\mathbf{k}+\mathrm{g}\mathbf{p}_\theta)|^2\, \widetilde{S}_s(\mathbf{k}+\mathrm{g}\mathbf{p}_\theta)}{(\sum_{\theta=\theta_1}^{\theta_3} |\widetilde{H}(\mathbf{k}+\mathrm{g}\mathbf{p}_\theta)|^2 + w)} \tag{8}$$

where g represents the three frequency orders g = -1, 0, 1, and w is another Wiener constant. The final SIM image $D_{SIM}(\boldsymbol{r})$ is obtained by performing an inverse Fourier transform of $\widetilde{D}_{\mathrm{SIM}}(\mathbf{k})$ multiplied by an apodization function to suppress high-frequency noise outside OTF's support.
The resolution amplification in SIM depends on the structured pattern's frequency $\boldsymbol{p}_\theta$; the closer it is to the cutoff frequency of the OTF, the higher the increment. With an appropriately chosen structured pattern, SIM can provide an enhancement in resolution up to a factor of two, although if the non-linear response of a sample can be exploited the resolution increase can be even higher.

1.2. FPM principle

In conventional transmission microscopy, a point source generates a plane wave of light which interacts with a semi-transparent object and becomes diffracted in a cone of light. Only part of the diffracted light is captured by the limited aperture of the microscope's objective, which results in a blurry image once it is recorded by the camera. FPM uses multiple light sources that illuminate the sample from various angles to allow different regions of the scattered cone of light to pass through the system's objective. In the frequency domain, a tilted illumination angle causes a shift of the sample's Fourier spectrum. By acquiring multiple images corresponding to different illumination angles and merging their respective bandpass-limited frequency domains, a larger frequency spectrum can be constructed. Transforming this spectrum to the spatial domain will result in a high-resolution (HR) image [3].
The use of an LED array as a light source, with varying angles of illumination, generates the effect of a synthetic NA given by the largest angle of illumination. As a consequence, the resolution amplification achieved by FPM will be limited by this synthetic NA_{ill} and the NA of the objective, NA_{obj}. The final expression for the resolution is given by (9):

$$R = \frac{\lambda}{NA_{ill} + NA_{obj}} \tag{9}$$

While traditional techniques sacrifice the field of view (FOV) to improve the resolution, FPM can result in a HR image that conserves the large FOV given by the low magnification objective, as the reconstruction can be done in segments that can later be merged together.
To achieve the optimal HR image reconstruction two sampling criteria must be fulfilled: there should be no pixel aliasing and a certain overlap between frequency spectra from images acquired from adjacent LEDs is required [4]. Pixel aliasing takes place when the resolution of a digital microscope is limited by the camera instead of the objective. In such case, $R_{cam} < 1$, R_{cam} being the sampling ratio of a digital microscope, defined by (10),

$$R_{cam} = \frac{f_{cam}}{f_{obj}} = \left(\frac{Mag}{2\Delta x_{cam}}\right) \Big/ \left(\frac{\mathrm{NA}}{\lambda}\right) \tag{10}$$

where Δx_{cam} is the detector's pixel size and Mag the objective's magnification.
For the second condition, the overlap between frequency spectra is defined by (11),

$$R_{overlap} = \frac{1}{\pi}\left[2\arccos\left(\frac{f_{LED}}{2f_{obj}}\right) - \frac{f_{LED}}{f_{obj}}\sqrt{\left(1-\left(\frac{f_{LED}}{2f_{obj}}\right)^2\right)}\right] \tag{11}$$

where $f_{LED} = \frac{1}{\lambda}\frac{D_{LED}}{\sqrt{(D_{LED})^2+h^2}}$ represents the frequency of the minimum tilted illumination angle, for a height between the sample and the LED array of h and a distance between LED elements given by D_{LED}. As a consequence, in a given experimental setup the overlap can be adjusted by varying the distance between neighboring LEDs, as well as the height from the sample to the LED array. Generally, higher overlap percentages correspond to better reconstruction results, although the effective NA is reduced. For cases in which $R_{cam} > 1$ the minimum overlap value was found to be 32% [4], but if there is aliasing and $R_{cam} < 1$ more spectrum overlap is required to achieve good reconstruction fidelity.

2. Method

2.1. Experimental setup (SIM)

Sensofar's S neox 3D profiler was used to acquire all the necessary experimental data, without any hardware modifications. The S neox system uses LEDs as a light source, which are collimated and directed onto a Microdisplay based on a digital micromirror device (DMD). The DMD consists of a diamond mirror array, where each mirror is switchable and has two stable positions at -12º and 12º (also called off and on states) which allows to steer the light and create illumination patterns. The structured patterns were created from scratch as bmp images that were read and transformed into micromirrors' on/off configurations. In particular, the patterns were created in two different orientations: $\theta_1 = 45°$ and $\theta_2 = 135°$. To achieve three different phases for each orientation the micromirror configuration was set to be one mirror on, two off. In total, six images were acquired for each set of data.

The pitch of each mirror was 7.64 μm; when projected onto the sample the period of the sinusoidal pattern was 0.36 μm, which corresponds to a frequency of 2.78 μm^{-1} in reciprocal space.

The objective used for all acquisitions was a 150x 0.9NA objective. While maintaining a constant NA, it was possible to acquire sets of data with different OTF width by changing the wavelength of the light source. Three wavelengths were used 460 *nm*, 532 *nm* and 632 *nm*, with respective OTF cutoff frequencies of 3.91 μm^{-1} , 3.38 μm^{-1} and 2.85 μm^{-1}.

2.2. SIM reconstruction algorithm (SIM-RA)

Six raw images are processed following the steps presented in the introduction and according to the algorithm overview shown in A 1. After applying a Fourier transform, the illumination spatial frequency $\boldsymbol{p}_\theta$ is estimated from the peaks of the Fourier transform. The resulting value must be equal to the value obtained by considering the pitch of the micromirrors and calculating the corresponding frequency. An inaccurate estimation can lead to reconstruction errors, as $\boldsymbol{p}_\theta$ will determine the shift needed to move each frequency component to its correct position in frequency domain.

Given that the illumination patterns have been created from scratch, their orientation and phase difference is perfectly known. Nevertheless, the phases must be optimized through a minimization function to correct any offset during the unmixing of frequencies.

Once unmixed, a Wiener filter is applied to different frequency components to reduce the inherent noise coming from the raw data while maintaining the resolution amplification. Next, the components are shifted to their correct location in the Fourier domain. The Fourier shift theorem must also be applied to the OTF, as shifted OTF spectra are required for the final reconstruction using the generalized Wiener filter. It is worth noting that a theoretical OTF has been used in the SIM-RA, which may be different from the real but unknown OTF. To simulate a more realistic behavior, the different OTF components are multiplied by an attenuation function, to simulate a faster decay near the cutoff frequency.

The reconstruction is complete once the generalized Wiener filter is applied, by merging all frequency regions through weighted sums. The spectrum is then multiplied by an apodization function in the form of an OTF mask using a Euclidean distance transform. Finally, both are inverse Fourier transformed to recover the SIM super-resolved image.

2.3. FPM experimental setup

An experimental FPM setup was built by replacing the light source of an S neox Five Axis 3D optical profiler with an 8 x 8 LED array with a pitch of 8 mm, controlled by an Arduino Nano board. The blue LEDs had a central wavelength of 470 nm and a bandwidth of 10 nm. The sample was placed above the LED array at three different heights to image using a 5x 0.15NA objective. The images were captured through transmission with the S neox camera, with a pixel size of 3.45 μm. Said camera was also connected to the Arduino board to synchronize the camera's acquisition exposure time and the LEDs illumination exposure time through a customized software.

To accommodate for the light source working through transmission and not reflection a special enclosure was 3D printed, which held the sample above the LED board at a height that could be adjusted. This structure also allowed to align the sample with the middle of the four central LEDs. The base of the structure was attached to a tip-tilt, which allowed to level the sample to leave it flat

and prevented the whole structure from moving in between measurements. The complete setup can be seen in Figure 1.

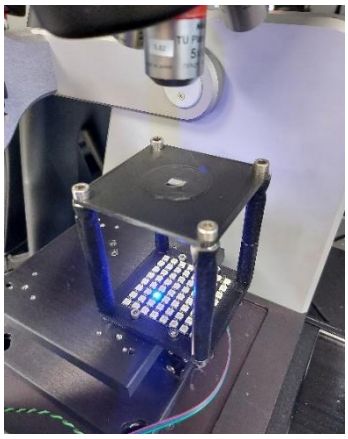

Figure 1. FPM experimental setup.

Stray light must be avoided in FPM as it can be the cause of artifacts in the reconstruction. To assure that no environmental light was affecting the experiment, the S neox system was covered with protective covers made of a dense and opaque material, which allowed to acquire the measurements in complete darkness. Additionally, for every data set an image was captured with no LEDs on, to be subtracted from every measurement as noise.
All LEDs were turned on sequentially at the defined exposure time, resulting in sets of 64 low-resolution (LR) images, saved in a bmp format.

2.4. FPM reconstruction algorithm (FPM-RA)

The FP algorithm is based on an iterative phase retrieval process by which it is possible to recover the phase from intensity measurements by setting two constraints: an intensity constraint in the spatial domain and an aperture constraint in the Fourier domain. An alternating projection is made between both constraints until the solution converges. These constraints are non-convex, meaning that the starting point determines whether the solution converges to a global or a local minimum. An overview of the FPM reconstruction procedure is shown in Figure 2.

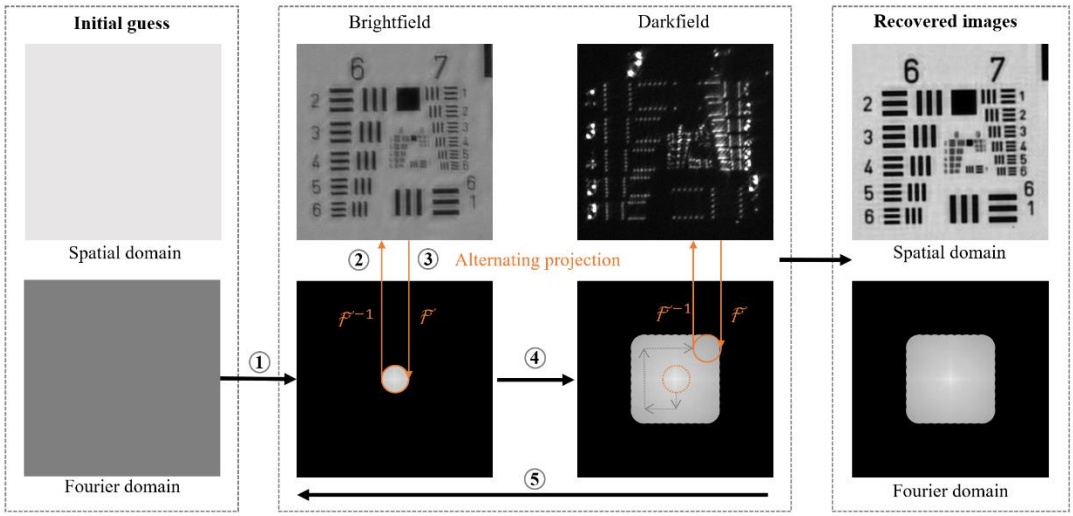

Figure 2. FPM recovery process overview: (1) Provide an initial guess of the HR image and its Fourier domain. (2) Aperture constraint: select a subregion of the Fourier domain corresponding to a particular angle of illumination and apply an inverse FT to generate a LR target image. (3) Intensity constraint: update the amplitude of the LR target image with the amplitude of an experimental LR acquisition under the same illumination angle and apply a FT to update the HR Fourier domain. (4) Repeat steps 2-3 for all illumination angles. (5) Repeat steps 2-4 until convergence.

The initial guess for the object is a constant array and the initial guess for the pupil is a coherent transfer function, which is a constant circular pupil with zeroes outside a radius $NA\,k_0$. One LR image can also be used as object initial guess.
Additionally, aberration recovery can be performed in FPM by making use of a method called embedded pupil recovery (EPRY) [5]. In this method, the pupil is updated alongside the object's frequency spectrum. The FPM-RA includes both options, performing two reconstructions. The overview of the FPM-RA is shown in A 2.

3. Results and discussion

Two of the samples used to acquire experimental data needed for the reconstruction algorithms were provided by Ceramic Data Solutions, consisting of glass samples with a sapphire substrate. Patterns were engraved on the glass by laser etching. The sample used for SIM contained arrays of point-like structures of different density gaps and sizes, ranging from 250 *nm* to 100 *nm*. For FPM the second sample was used, which contained larger structures (~1 μm), more appropriate to image with a low magnification objective. Additionally, a Ronchi Ruling Glass slide was used to acquire data for SIM-RA. The Ronchi slide is a periodic sample with a 3600 lp/mm pattern frequency, resulting in a resolution of 278 nm.
The performance of SIM-RA was evaluated by visually comparing the reconstructed image with the brightfield and the confocal images, which were readily obtained from the raw data. Confocal images provide high contrast, allowing for a good comparison with SIM images. The profiles from the same spatial regions were also analyzed.
From the first sapphire sample four different arrays were imaged and processed by SIM-RA. The central regions of two arrays, corresponding to 200 nm and 100 nm structures, are represented on the Figure 3 and Figure 4, respectively.

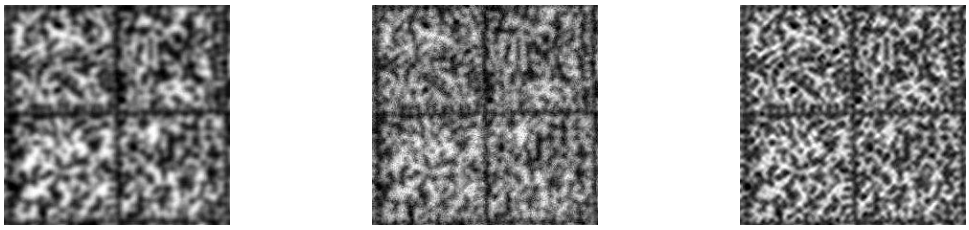

(a) (b) (c)

Figure 3. Comparison between a (a) brightfield, (b) confocal and (c) SIM image, for 200 nm structures.

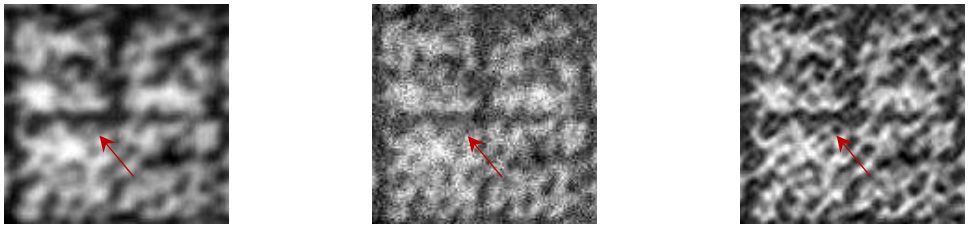

(a) (b) (c)

Figure 4. Comparison between a (a) brightfield, (b) confocal and (c) SIM image, for 100 nm structures.

The central wavelength of the LED used to acquire the raw data was 532 nm, which corresponds to a resolution of 295 nm. After the SIM-RA the OTF's width is increased up to 80%, resulting in a new resolution of 162 nm. For the case represented on Figure 3, the spatial frequency of the structures was relatively close to the cutoff frequency. The SIM-RA shows an improvement in image quality by amplifying the contrast of the highest spatial frequencies, which appear less contrasted and nosier on the brightfield and confocal images. For the second case, shown on Figure 4, the resolution of the 100 nm structures is still outside the new OTF's support. Due to this fact, not all structures are completely resolved but an improvement in resolution can be seen regardless. The three red arrows point to circular structures that were not apparent on the brightfield and confocal images but that can be distinguished in the SIM image.

To further see the improvement in resolution, a profile has been traced across the same region of a brightfield and SIM reconstructed image of a 100 nm structure array, as seen on Figure 5.

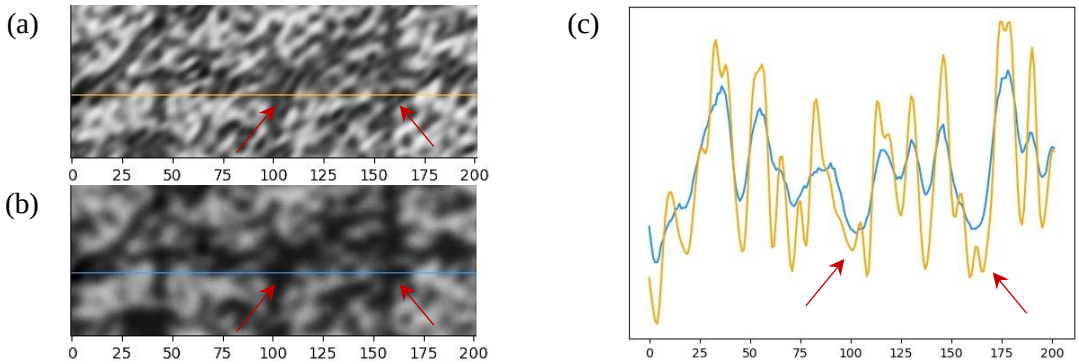

Figure 5. 100 nm structures, comparison between a (a) reconstructed SIM image region with a (b) brightfield image region. The corresponding profile is shown in (c).

Judging from Figure 5, the contrast is clearly improved in the SIM image as shown by the scale of the graph on the right. The resolution is also better, as the SIM profile differentiates between two separate structures where only one was seen before, as is shown by the red arrows.
For the case of the Ronchi slide, the structured patterns were projected in only one direction, to achieve maximum alignment with the natural features of the sample and thus more clearly visible Moiré fringes, resulting in sets of only three images being captured. Figure 6 shows the reconstruction for an acquisition done by projecting the patterns with a wavelength of 532 nm.

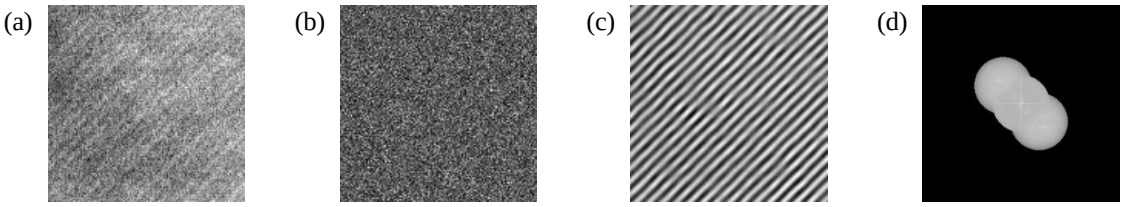

Figure 6. 64 x 64 px region of a 3600 lp/mm Ronchi slide, (a) brightfield, (b) confocal, (c) SIM image and (d) extended frequency spectrum of the reconstructed image shown in (c).

The natural frequency of the sample is 3.6 μm^{-1}, slightly above the theoretical cutoff frequency; the fact that some structure can be seen on the brightfield image from Figure 6 means that the cutoff of the real OTF may be slightly larger than the calculated. Nevertheless, the OTF is greatly attenuated for this frequency and as a consequence the contrast is very low. The confocal image does not show any detail, which could be due to a suboptimal axial focus position. The acquisition of the raw data was performed selecting the focus position that maximized the contrast of Moiré fringes, which may differ to some degree with the focus of the surface for different wavelengths. Despite this, the reconstructed image perfectly shows the inherent frequency of the Ronchi slide. This frequency can be seen as two peaks on the extended frequency spectrum.
To further evaluate the performance of SIM-RA, the obtained results were compared with an open-source reconstruction algorithm, provided as a plugin in the ImageJ software, called fairSIM. The performance against fairSIM was tested both with the sapphire and the Ronchi samples. The results are represented on Figure 7.

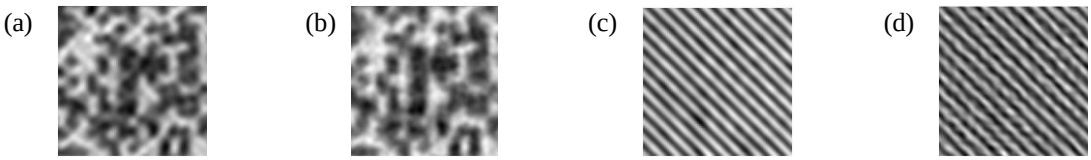

Figure 7. Sapphire sample and Ronchi slide by SIM-RA (a), (c) and fairSIM (b), (d).

The results given by both algorithms are very similar, with slightly better results for the case of the Ronchi slide reconstructed by SIM-RA, as the fringes appear more even.

The final SIM reconstructions, although showing an enhancement in resolution, are not artifact free. This is particularly evident for the sapphire sample, where the reconstructed image still appears blurry and with ringing artifacts.
The fidelity of SIM is often put into question, as this technique is prone to artifacts and it requires extensive parameter optimization to achieve an artifact-free result. Some parameters are estimated from the experimental data, such as the structured pattern frequency and phases, while other parameters must be adjusted by the user by trial and error, such as the three Wiener constants. The reconstruction fidelity relies on an accurate election of these parameters, as an incorrect estimation can lead to additional artifacts, but they greatly depend on the sample type and must be adjusted for each reconstruction even if the sample is unchanged. Results in this thesis use the parameters found following extensive experimentation, although further optimization may be possible by applying the guidelines presented in articles centered around parameter optimization [6].
The second sapphire sample was used to evaluate the performance of the FPM-RA, in conjunction with open-source data [7]. Said data was acquired with a 4x 0.1 NA objective, with an LED pitch of 4 mm and a sample placed at a height of 67.5 mm, resulting in an overlap of 63% and a 0.33 effective NA. From the 293 images, the central set of 9 x 9 images of the USAF resolution test target were used to run FPM-RA. The results of the reconstruction can be seen on the Figure 8.

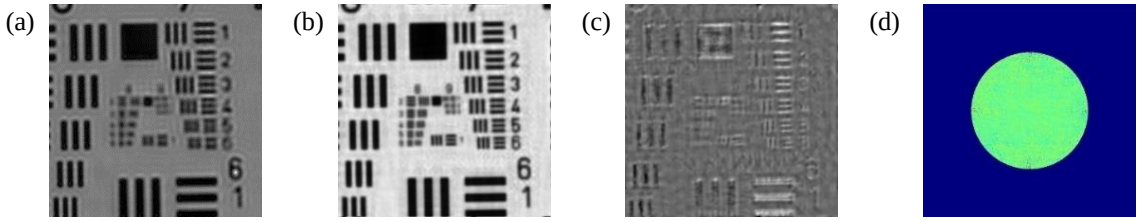

Figure 8. Reconstruction of a USAF resolution test target, 256 x 256 px region: (a) LR image, (b) reconstructed image, (c) recovered phase and (d) recovered pupil.

The best results were achieved by updating with EPRY, thus updating the pupil as well as the object spectrum. The recovered pupil appears almost constant, not showing any prominent aberration component. The phase appears less constant on areas that still had sapphire deposited on the glass, blocking the transmission of light, and appearing black on the LR image.
The reconstructed image, corresponding to an effective NA of 0.33, is able to show more detail when compared with the LR image. The central region, containing higher frequencies, has gone from appearing blurry to showing the orientation of the line pairs. The numbers that represent the different groups have also become sharper.
The same algorithm was applied to the experimental data coming from imaging the second sapphire sample; three sets of LR images corresponding to three heights were evaluated to see the effects of the overlap on the reconstruction. The results can be seen on the Figure 9.

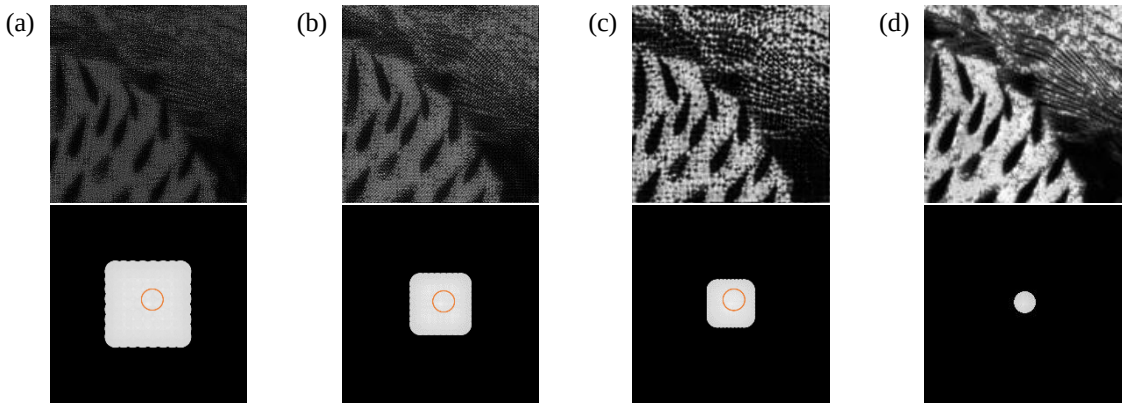

Figure 9. Reconstruction of a 128 x 128 px sapphire on glass sample, showing the HR image and the frequency spectrum for three cases: (a) h = 5 cm, op = 42%, eNA = 0.6 (b) h = 10 cm, op = 65%, eNA = 0.43 (c) h = 15 cm, op = 78%, eNA = 0.33 and (d) low resolution image for comparison, NA = 0.15. The parameters correspond to the height (h), overlap (op) and effective NA (eNA).

Although in all three cases the spectrum overlap is higher than the minimum 32% required for a FPM reconstruction, Figure 9 shows that small overlaps are not enough to converge on the correct result. If the convergence was correct, data acquired with smaller overlap would result in a higher effective NA, but from the previous image it can be seen that enough spectrum overlap is essential. The fact that not even an overlap of 65% gave the expected results may suggest that there was some degree of pixel aliasing in the raw images, as that would explain why even above the minimum overlap percentage the reconstruction is not optimal.
As was expected, the best result was achieved with the largest height difference between the sample and the LED array, and thus highest spectrum overlap. The theoretical effective NA in this case is 0.33, meaning that the original NA of 0.15 is doubled. The reconstruction result was compared with a ground truth acquired with a 10x 0.3NA objective, as it was the objective that should give the most similar results to the reconstructed image. A comparison between these images can be seen in the Figure 10.

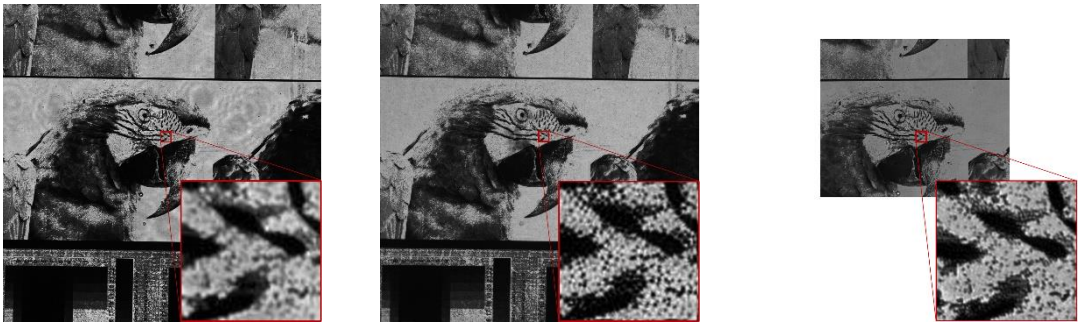

(a) (b) (c)

Figure 10. Comparison between the reconstruction and ground truth for zoomed in regions of 64 x 64 px, sapphire on glass: (a) LR image, (b) HR image (c) acquisition with a 10x 0.3NA objective (smaller FOV).

The reconstruction shown on Figure 10 proves an improvement in resolution when compared to the LR image, as the image appears sharper and it shows structures that were indistinguishable before. The HR image approaches the result acquired using a 10x objective, and with further optimization of the data acquisition process and computational reconstruction the HR image could potentially surpass said result, as the effective NA is superior.
For the experimentally acquired dataset the best results were achieved without EPRY, thus without updating the pupil. This could be because the recovery process was not able to correctly model the aberrations, and thus the initial guess is not accurate enough to make the algorithm converge on the correct pupil function.

4. Conclusions

In this thesis, the performance of two super-resolution techniques, SIM and FPM, has been explored by implementing them into already existing 3D optical profilers.
The first technique, more complex in terms of computer processing but easier to implement experimentally, showed an improvement in lateral resolution for a high magnification, 150x 0.9NA objective. Two sample types were used to run the algorithm; a periodic Ronchi slide, and a point-like sample filled with nanometric structures of varying size. Applying the SIM-RA algorithm to the Ronchi slide allowed to go from brightfield and confocal images where minimal detail was seen to perfectly visible periodic fringes of the expected period of 270 nm. The SIM-RA algorithm also improved the visibility of the nanometric structures of the second sample, increasing the resolution up to an 80% of the original limit, although the results were more affected by artifacts.
For the second technique, a structure was designed to acquire images in transmission mode by using multiple light sources. One experimental set of data was used to evaluate the algorithm's behavior, corresponding to a semi-transparent sapphire substrate sample, and a set of open-source images of the USAF resolution test target. Two paths were designed to be taken by the algorithm; one that updates the pupil together with the object frequency spectrum and one that only updates the spectrum. The first path showed better result for the open-source data, as these images may be free of aberrations. The second path resulted in a better reconstruction for the experimentally acquired images, although the spectrum overlap had to be very high for the algorithm to converge on a result.

The tested techniques were proven to show an improvement in lateral resolution, although further optimization is required. For the case of SIM, the reconstruction should be less user dependent, while for the FPM case the experimental setup must be improved to obtain high spectrum overlaps without sacrificing effective NA. Both issues will be explored in future work.

5. Acknowledgments

I want to express my gratitude to my supervisor Dr. Guillem Carles for his guidance and advice, to the R&D department for their support and to Ceramic Data Solutions for providing the samples used in this research project.

6. Appendix

Algorithm 1: SIM-RA

Input: System OTF $\tilde{H}(\mathbf{k})$ and six raw SIM images $D_{\theta,\phi}(\mathbf{r})$, corresponding to orientations $\theta = \theta_1, \theta_2$ and phases $\phi = \phi_1, \phi_2, \phi_3$
Output: Reconstructed SIM image $D_{SIM}(\mathbf{r})$

for $\theta = \theta_1, \theta_2$ **do**
  for $\phi = \phi_1, \phi_2, \phi_3$ **do**
    Apply Fourier Transform to obtain $\tilde{D}_{\theta,\phi}(\mathbf{k})$
    Estimate illumination spatial frequency $\mathbf{p}_\theta$ from $\tilde{D}_{\theta,\phi}(\mathbf{k})$
    Optimize illumination phase shift ϕ
  Apply equation (4) to obtain unmixed frequency components $\tilde{S}(\mathbf{k} + g\mathbf{p}_\theta)\tilde{H}(\mathbf{k})$, where g = -1, 0, 1
  Apply Wiener filter to central and side components given by equations (5) and (6) to obtain filtered components $\tilde{S}_u(\mathbf{k})$ and $\tilde{S}_u(\mathbf{k} \pm \mathbf{p}_\theta)$
  Use the Fourier shift theorem (7) to move each frequency component to its correct location in Frequency domain, obtaining $\tilde{S}_s(\mathbf{k} + g\mathbf{p}_\theta)$
  Apply the Fourier shift theorem to shift the OTF spectra $|\tilde{H}(\mathbf{k} + g\mathbf{p}_\theta)|^2$
Merge all frequency components by using a generalized Wiener filter, see equation (8)
Apply apodization function to reduce high-frequency noise outside the OTF support
Perform an inverse Fourier transform to recover the final SIM SR image $D_{SIM}(\mathbf{r})$

A 1. Overview of the SIM reconstruction algorithm.

Algorithm 2: FPM-RA

Input: LR acquired images $I_n^e(x, y)$ and incident wavevectors from LEDs (k_{xn}, k_{yn}), for incident angles $n = 1, ..., N$. Spectrum update sequence $G(n)$ as a clockwise spiral from the center to the edges.
Output: Recovered high resolution image $o(x, y)$ and pupil aberration $P(k_X, k_y)$

Define initial object spectrum and pupil guess, $O(k_x, k_y) = \mathcal{F}\{o(x, y)\}$ and $P(k_x, k_y) = circ(NAk_0)$
for i *iterations* **do**
  for n *in* $G(n)$ **do**
    $\varphi_n^e(k_x, k_y) = O(k_x - k_{xn}, k_y - k_{yn})\, P(k_x, k_y)$, aperture constraint
    $\phi_n^e(x, y) = \mathcal{F}^{-1}\{\varphi_n^e(k_x, k_y)\}$, low-resolution target image
    $\phi_n^u(x, y) = \sqrt{I_n^e(x, y)}\frac{\phi_n^e(x,y)}{|\phi_n^e(x,y)|}$, intensity constraint
    if *EPRY* **then**
      $\Delta\varphi_n = \mathcal{F}\{\phi_n^u(x, y)\} - \varphi_n^e(k_{xn}, k_{yn})$
      $O(k_x - k_{xn}, k_y - k_{yn}) = O(k_x - k_{xn}, k_y - k_{yn}) + \alpha\frac{|P(k_{xn},k_{yn})|P^*(k_{xn},k_{yn})}{|P(k_{xn},k_{yn})|_{\max}(|P(k_{xn},k_{yn})|^2+\delta_1)}\Delta\varphi_n$
      $P(k_{xn}, k_{yn}) = P(k_{xn}, k_{yn}) + \beta\frac{|O(k_x-k_{xn},k_y-k_{yn})|O^*(k_x-k_{xn},k_y-k_{yn})}{|O(k_x-k_{xn},k_y-k_{yn})|_{\max}(|O(k_x-k_{xn},k_y-k_{yn})|^2+\delta_2)}\Delta\varphi_n$
    else
      $\phi_n^e(k_x, k_y) = \mathcal{F}\{\phi_n^u(x, y)\}$ and $O(k_x - k_{xn}, k_y - k_{yn}) = O(k_x - k_{xn}, k_y - k_{yn}) + \phi_n^e(k_x, k_y)$
Recover $o(x, y) = \mathcal{F}^{-1}\{O(k_x, k_y)\}$

A 2. Overview of the FPM reconstruction algorithm.

7. References

[1] M. G. L. Gustafsson, «Surpassing the lateral resolution limit by a factor of two using structured illumination microscopy,» *Journal of Microscopy*, vol. 198, pp. 82-87, 2000.

[2] A. Lal, C. Shan and P. Xi, "Structured Illumination Microscopy Image Reconstruction Algorithm," *IEEE Journal of Selected Topics in Quantum Electronics*, vol. 22, p. 50–63, 2016.

[3] G. Zheng, Fourier Ptychographic Imaging: A Matlab Tutorial, Morgan & Claypool Publishers, 2016.

[4] J. Sun, Q. Chen, Y. Zhang and C. Zuo, "Sampling criteria for Fourier ptychographic microscopy in object space and frequency space," *Opt. Express*, vol. 24, pp. 15765-15781, 2016.

[5] X. Ou, G. Zheng and C. Yang, "Embedded pupil function recovery for Fourier ptychographic microscopy," *Opt. Express*, vol. 22, pp. 4960-4972, 2014.

[6] C. Karras, M. Smedh, R. Förster, H. Deschout, J. Fernandez-Rodriguez and R. Heintzmann, "Successful optimization of reconstruction parameters in structured illumination microscopy – A practical guide," *Optics Communications*, vol. 436, pp. 69-75, 2019.

[7] L. Tian, X. Li, K. Ramchandran and L. Waller, "Multiplexed coded illumination for Fourier Ptychography with an LED array microscope," *Biomed. Opt. Express*, vol. 5, pp. 2376-2389, 2014.